

Sampling and Inference of Networked Dynamics using Log-Koopman Nonlinear Graph Fourier Transform

Zhuangkun Wei¹, Bin Li², Chengyao Sun³, Weisi Guo^{1,3,4*}

Abstract—Monitoring the networked dynamics via the minimum subset of nodes is essential for a variety of scientific and operational purposes. When there is a lack of an explicit model and networked signal space, traditional evolution analysis and non-convex methods are insufficient. An important data-driven state-of-the-art method uses the Koopman operator to generate a linear evolution model for a vector-valued observable of original state-space. As a result, one can derive a sampling strategy via the linear evolution property of observable. However, current polynomial Koopman operators result in a large sampling space due to: (i) the large size of polynomial based observables ($O(N^2)$, N number of nodes in network), and (ii) not factoring in the nonlinear dependency between observables.

In this work, to achieve linear scaling ($O(N)$) and a small set of sampling nodes, we propose to combine a novel Log-Koopman operator and nonlinear Graph Fourier Transform (NL-GFT) scheme. First, the Log-Koopman operator is able to reduce the size of observables by transforming multiplicative poly-observable to logarithm summation. Second, a nonlinear GFT concept and sampling theory are provided to exploit the nonlinear dependence of observables for Koopman linearized evolution analysis. Combined, the sampling and reconstruction algorithms are designed and demonstrated on two established application areas. The results demonstrate that the proposed Log-Koopman NL-GFT scheme can (i) linearize unknown nonlinear dynamics using $O(N)$ observables, and (ii) achieve lower number of sampling nodes, compared with the state-of-the-art polynomial Koopman linear evolution analysis.

Index Terms—network dynamics, sensor placement, Koopman operator, Graph Fourier Transform, compression

I. INTRODUCTION

Many engineering, social, and biological complex systems consist of dynamical elements connected via a large-scale network. These include both explicit [1], [2] and latent dynamics, spanning: urban structure [3], social networks [4], economics [5], engineering infrastructure [6], ecology [7], biology clocks [8], epidemic spreading [9], and organizational structure [10].

Collecting data on networks is important for a variety of scientific and practical reasons, ranging from scientific model development to Digital Twin informed maintenance [11], [12]. However, when the size of the network is large, as is the case for national infrastructure, gene regulatory networks, or social networks; effective monitoring through a small subset of critical nodes is essential.

¹University of Warwick, UK. ²Beijing university of Posts and Telecommunications, Beijing, China. ³Cranfield University, UK ⁴The Alan Turing Institute, UK. *Corresponding Author: weisi.guo@cranfield.ac.uk.

A. Literature Review

In classic topology-centric analysis, the influential nodes are often determined using eigen analysis resulting in wide measures such as PageRank centrality. However, when the dynamics are also important, the relationship between topological influence and cascade dynamics is unclear [13]. When nonlinear dynamics is coupled with complex networks, current methods fall into two categories. First, reduced order models (e.g. heterogeneous mean field around equilibrium conditions [14]) cannot well approximate cascade transient dynamics. This means we can only understand the equilibrium conditions and the impact of perturbations.

1) *Model Driven*: In order to achieve transient behaviour understanding (also known as graph observability), a well-studied group of schemes is state-based reconstruction. Popular methods include convex optimisation [15], causal modeling [16], and linear evolution analysis (e.g., checking rank conditions of the linear model that maps initial state to all forward states, or maximizing energy of sampled states computed by model-relevant observability gramians) [17]–[21]. These approaches all provide attractive performances on sampling node compression and state recovery accuracy, under the important premise of a known and linear/linearized underlying model. Their drawback is the inability to address the sampling and recovery challenges in the absence of dynamic equations.

2) *Data Driven*: Instead of relying on explicit dynamic equations, an alternative group resorts to the prior knowledge of the signal-space [11]. The methods include sparsity and spectral analysis. For instance, the compressed sensing (CS) schemes [22], [23] selected the sampling nodes by analyzing the principal components. Graph sampling methods [17], [24]–[33] determine a sampling node set for signals that belong to a sub-space (referred to as band-limited) of a Graph Fourier Transform (GFT) operator (e.g., Laplacian [24]–[30], joint time-graph Fourier transform [33], and data-driven [11] operators). One obvious disadvantage lies in the signal-dependent sampling nodes selection and recovery process, which is not suitable for different signal-space caused by perturbations with significantly different spectral characteristics. As such, there is a strong demand to design (i) **signal-independent** network sampling and recovery schemes, (ii) **in the absence of explicit dynamic equations**.

3) *Koopman Operator*: To address the aforementioned signal-independence and unknown dynamic models, another set of approaches relies on the Koopman operator [34]–[38], which is a linear but infinite dimensional operator that governs

the evolution of scalar-value observables (functions) defined on the state space of a nonlinear dynamical system. In the context of network signal processing (with N nodes), the work in [37] developed a polynomial-based Koopman operator for dynamics linearization, by selecting the observables as the $M = O(N^2)$ key polynomial terms of Taylor series (e.g., the multiplicative terms of node 1 and node 2, $x_1 \cdot x_2$). Then, their further work in [38] derived a minimum number of sampling nodes, by treating the observable set as \mathbb{R}^M and using linear evolution analysis (which maps the sampling nodes to the leading eigenvectors of the Koopman observability gramian). However, the scheme has two drawbacks. First, to ensure linearization accuracy, the polynomial-based Koopman operator leads to a size explosion ($O(N^2)$) when addressing large-scale networks (see Figs. 5-6). Second, the direct use of linear evolution analysis (e.g., rank and gramian analysis) on observable overlooked the intrinsic nonlinear relations between observables, which are all determined by the originally lower sized state space (e.g., $x_1, x_2, x_1x_2, x_1^2x_2^2$ are all observables for polynomial-based Koopman linearized model, but are determined by original networked data x_1 and x_2). This will result in extra redundant sampling nodes for signal recovery. We will explain this in greater detail in Section V. A, and in Figs. 5-6.

B. Contributions & Organization

In this work, we propose a novel logarithm-based Koopman and non-linear GFT scheme (abbreviated as Log-Koopman NL-GFT) for sampling and recovering the large-scale networked data. The detailed contributions are listed in the following, each addressing an aforementioned shortfall in current approaches:

(1) We propose a logarithm based Koopman operator to linearize the unknown nonlinear networked dynamics. Here, the logarithm-form observables of original state-space are designed to approximate the multi-element multiplicative terms of Taylor series by logarithm summation. In this view, the size of observables can be reduced to $O(N)$, as smaller number of logarithm terms can be used and linearly combined for large number of polynomial-based observables in [37]. This suggests the ability of the proposed Log-Koopman to prevent the size explosion when linearizing large-scale networked data.

(2) We combine the linearization ability of the Log-Koopman operator with a novel nonlinear GFT, by exploiting the nonlinear dependence between the M observables that are defined on the lower size of N original state-space. As such, the proposed Log-Koopman NL-GFT sampling and recovery scheme is able to combine the linear evolution property with nonlinear dependency between observable, thereby outperforming the scheme [37] that only relies on linear evolution analysis on the Koopman linearized model. Also, other than a signal-space dependent bandlimited property of linear GFT [17], [24]–[33], the nonlinear GFT captures the signal-space independent relations of observables, thereby capable of obtaining a signal-independent sampling node set.

(3) We evaluate our proposed Log-Koopman NL-GFT sampling and recovery scheme via two different application

domains: (a) networked Biochemical Dynamics of protein-protein interactions, and (b) networked gene Regulatory Dynamics. The results demonstrate that (i) the proposed Log-Koopman operator is able to reduce the observable size to $O(N)$ as opposed to $O(N^2)$ of Poly-Koopman in [37], and (ii) the proposed nonlinear GFT scheme can reduce the number of sampling nodes, compared with the direct use of linear evolution analysis in [38] after the derivation of Koopman linearized model. This suggests a promising prospect of the proposed Log-Koopman NL-GFT sampling and recovery scheme to a wide range of scientific and engineering monitoring applications.

The rest of this paper is structured as follows. In Section II, we detail the networked nonlinear dynamical system and the problem formulation. In Section III, we provide our designed logarithm based Koopman operator. In Section IV, we elaborate the nonlinear GFT concept and theory. Then, a greedy algorithm for sampling node selection and a gradient descend algorithm for recovery are provided. In Section V, we theoretically compare our proposed Log Koopman NL-GFT scheme with other state of the art approaches. Section VI gives the data-driven experiments and performance discussion. In Section VII, we finally conclude the paper and discuss potential future areas of research.

II. MODEL AND PROBLEM FORMULATION

A. Networked Dynamic Model

The networked dynamic is described by its underlying graph topology and the dynamic data flow over it. The network topology is configured by a static graph, denoted by $\mathcal{G}(\mathcal{N}, \mathbf{A})$. Here, $\mathcal{N} = \{1, \dots, N\}$ represents a set of node subscripts. \mathbf{A} of size $N \times N$ is the binary adjacent matrix, in which the (i, j) th element $a_{i,j} \in \{0, 1\}$ reflects the existence of link from node j to node i .

Given the topology of the network, the dynamic data over each node evolves in accordance with its self-dynamic and the coupling interactions from its adjacent nodes. By denoting the data for each $t \in \mathbb{N}^+$ discrete time as a vector of size $N \times 1$, i.e., $\mathbf{x}_t = [x_{1,t}, \dots, x_{N,t}]^T$, such evolution can be expressed as:

$$\mathbf{x}_{t+1} = \mathbf{F}(\mathbf{x}_t, \mathbf{A}), \quad (1)$$

where $\mathbf{F} : \mathbb{R}^N \rightarrow \mathbb{R}^N$ is an unknown combined self and coupling nonlinear operator that evolves t th state to $(t+1)$ th state via the adjacent matrix \mathbf{A} . At $t = 1$, we regard $\mathbf{x}_1 \in \mathbb{R}^N$ as an external input, which is also unknown.

B. Problem Formulation

The purpose of this work is to reconstruct the networked dynamical data via a subset of sampling nodes' data. To be specific, given the sampling node set $\mathcal{S} = \{n_1, \dots, n_S\} \subset \mathcal{N}$, we define the sampling matrix of size $S \times N$ with elements:

$$\mathbf{S} = [s_{i,j}], \text{ with } s_{i,n_i} = 1, s_{i,j \neq n_i} = 0. \quad (2)$$

Then, the samples collected from the sampling nodes are: $\mathbf{S} \cdot \mathbf{x}_{t+1}$. As such, given the monitoring discrete time-span as $t \in \{1, \dots, \tau\}$, the aim is to find the sampling node set \mathcal{S} and to

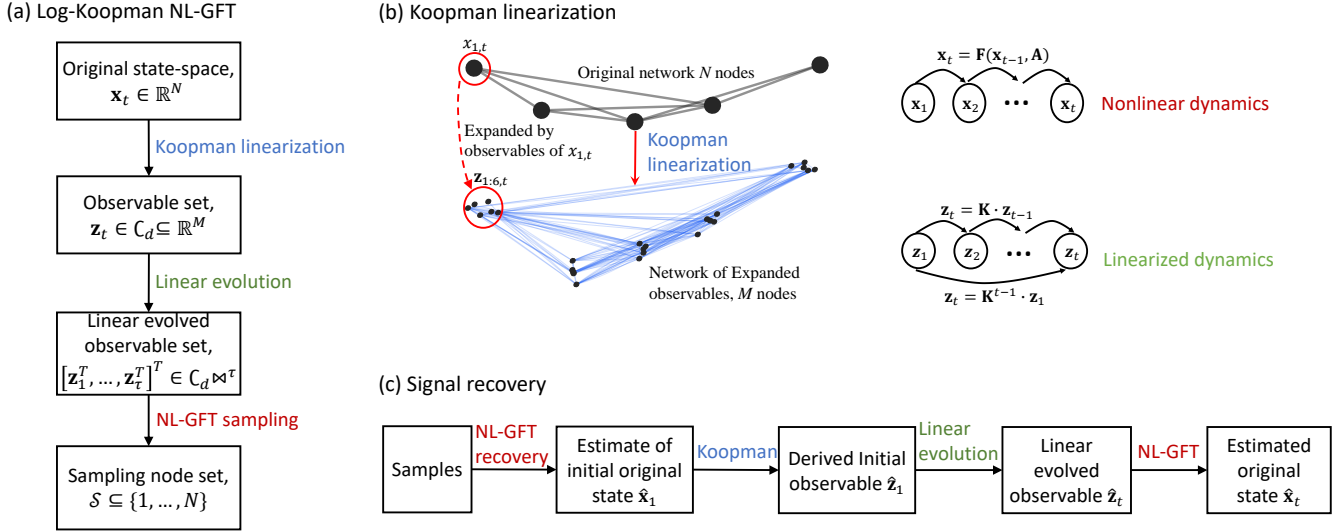


Fig. 1. Schematic flow of the proposed Log-Koopman NL GFT sampling and recovery method. (a) illustrates the sampling process. (b) shows Koopman linearization, which generates a linear evolution model of extended size $M = O(N)$ observables on original state-space of size N . (c) gives the recovery process.

design the recovery process to reconstruct $\mathbf{x}_{1:\tau} = [\mathbf{x}_1, \dots, \mathbf{x}_\tau]$ via the samples $\mathbf{S} \cdot \mathbf{x}_{1:\tau}$.

As aforementioned, the challenges on the design of sampling and recovery methods lie in the absences of both the evolution model \mathbf{F} in Eq. (1), and the signal-space (i.e., a subspace of \mathbb{R}^N), which make existing works on equation-driven graph observability [17]–[21], and signal-space dependent compression approaches [17], [24]–[33] less attractive. As such, this motivates our work to 1) approximate a linear evolution model, and 2) find orthogonal nodes for data sampling and recovery.

C. Sketch of Design

The sketch of the design of sampling and recovery scheme is illustrated via Fig. 1. We firstly adopt the Koopman theory to linearize the unknown nonlinear networked data. Then, the concept and theory of nonlinear GFT will be proposed and used for sampling node selection and signal recovery. We will elaborate them in the following sections.

III. KOOPMAN OPERATOR AND LINEARIZATION

A Koopman operator of one dynamical system is a linear operator that evolves the selected observable functions of the state space as the time advances. By defining the space of all observable functions as \mathcal{F} , and stacking such observable functions as $\psi = [\psi_1, \dots, \psi_M]^T$ with $\psi_m \in \mathcal{F} : \mathbb{R}^N \rightarrow \mathbb{R}$ and $m \in \{1, \dots, M\}$, the Koopman operator is specified as [34], [37], [38]:

$$\mathcal{K}\psi(\mathbf{x}_t) = \psi(\mathbf{F}(\mathbf{x}_t)) = \psi(\mathbf{x}_{t+1}). \quad (3)$$

As such, by selecting appropriate observable functions, one could derive the Koopman operator, and use it as an equivalent evolution model for the corresponding non-linear dynamic system.

A. State-of-the-art Polynomial-based Koopman Operator

It is noteworthy that one main difficulty lies in the infinite dimension of \mathcal{F} , i.e., $M \rightarrow +\infty$, which makes the Koopman operator \mathcal{K} infinite, and thereby impractical in real-world systems. To address it, many works [34], [37], [38] tried to approximate the Koopman operator, by using definite observable functions and span them as the approximated observable space: $\mathcal{F}_D \subset \mathcal{F}$. Specially, the work in [37] selected from a proven complete of observable function space leveraged on the polynomial terms of Taylor expansion, i.e., [37]

$$\mathcal{F} = \left\{ \prod_{i=1}^N x_{i,t}^{p_i}, \forall p_i \in \mathbb{N} \right\}. \quad (4)$$

By selecting $\psi(\mathbf{x}_t) = [x_{i,t}^{p_i} \cdot x_{j,t}^{p_j}]^T$ with $\forall i, j \in \mathcal{N}$, $p_i, p_j \in \{0, 1, 2\}$, they constructed the approximated Koopman operator for small-scale (i.e., $N < 10$) networked dynamic linearization. However, for large-scale networks ($N > 50$), in order to maintain the linearization accuracy, the scheme leads to a size explosion of observables by selecting complex multi-element multiplicative basic functions (e.g., $x_{i,t}^{p_i} \cdot x_{j,t}^{p_j} \cdot x_{m,t}^{p_m} \cdot x_{n,t}^{p_n}$). We explain this by showing how the multi-element multiplicative terms contributes to the existing observable functions in [37], i.e.,

$$\begin{aligned} x_{i,t} \cdot x_{j,t} &= f_i(\mathbf{x}_{t-1}) \cdot f_j(\mathbf{x}_{t-1}) \\ &= \sum_{\substack{m,n \in \mathcal{N} \\ p_i, p_j, p_m, p_n \in \{0,1,2\}}} \alpha_{i,j,m,n} \cdot x_{i,t-1}^{p_i} \cdot x_{j,t-1}^{p_j} \cdot x_{m,t-1}^{p_m} \cdot x_{n,t-1}^{p_n}, \end{aligned} \quad (5)$$

where $\alpha_{i,j,m,n}$ denotes the weight. As is illustrated in Eq. (5), the number of 4-element multiplicative terms is increasing with the increase of network scale N . Therefore, in order to keep the accuracy of the Koopman linearization, one have to expand the selected observable function set $\psi(\mathbf{x}_t)$ that covers such terms. This will lead to a size of $> N^2$ size

increase for the approximated Koopman operator, which if used for large-scale network (e.g., $N > 50$), may cause heavy computational burden for further sampling selection and signal recovery processes.

B. Logarithm-based Koopman Operator

To address the aforementioned size explosion, we design a novel group of observable functions that can transform the multiplicative terms (e.g., $x_{i,t}^{p_i} \cdot x_{j,t}^{p_j}$) into summation terms. The idea is to leverage on the following logarithm approximation, i.e.,

$$\begin{aligned} \log(1+x) + \log(1+y) &= \log((1+x)(1+y)) \\ &\approx xy + x + y, \end{aligned} \quad (6)$$

when $x, y \in (0-\delta, 0+\delta)$ with a small δ . As such, by assigning a large constant C such that $\sup\{x_{i,t}/C, i \in \mathcal{N}, t \in \mathbb{N}^+\} < \delta$, we design the vector-valued observable function as:

$$\boldsymbol{\psi}(\mathbf{x}_t) = \left[1, \frac{x_{i,t}}{C}, \log\left(1 + \left(\frac{x_{i,t}}{C}\right)^{p_i}\right) \right]^T, \quad \forall i \in \mathcal{N}, \quad (7)$$

with some $p_i \in \mathcal{P} \subset \mathbb{N}$. Also, we write the vector-valued observable of size $M \times 1$, with its range set $\mathcal{C}_d \subset \mathbb{R}^M$ as:

$$\mathbf{z}_t = \boldsymbol{\psi}(\mathbf{x}_t), \quad \mathbf{z}_t \in \mathcal{C}_d \subset \mathbb{R}^M. \quad (8)$$

Given Eq. (7), we show in the following that each observable function at time t can be evolved and approximated by the summation of others at time $t-1$. The observable function $x_{i,t}/C$ is expressed by:

$$\begin{aligned} \frac{x_{i,t}}{C} &= \frac{f_i(\mathbf{x}_{t-1})}{C} \\ &= \frac{1}{C} \left(f_i(\mathbf{0}) + \mathbf{x}_{t-1}^T \nabla f_i(\mathbf{0}) + \frac{1}{2} \mathbf{x}_{t-1}^T \mathbf{H}_{f_i}(\mathbf{0}) \mathbf{x}_{t-1} + o^n \right) \\ &= \frac{f_i(\mathbf{0})}{C} + \sum_{\substack{m,n \in \mathcal{N} \\ p,q \in \mathcal{P}}} a_{m,n,p,q} \cdot \left(\frac{x_{m,t-1}}{C}\right)^p \cdot \left(\frac{x_{n,t-1}}{C}\right)^q \\ &\approx \frac{f_i(\mathbf{0})}{C} + \sum_{m \in \mathcal{N}} a_m \frac{x_{m,t-1}}{C} + \sum_{\substack{m \in \mathcal{N} \\ p \in \mathcal{P}}} \log\left(1 + \left(\frac{x_{m,t-1}}{C}\right)^p\right), \end{aligned} \quad (9)$$

where the function $f_i(\cdot)$ is the i th element of $\mathbf{F}(\cdot)$, $\nabla f_i(\cdot)$ is its gradient function, $\mathbf{H}_{f_i}(\cdot)$ is its Hessian matrix. $a_{m,n,p,q}$ and a_m are coefficients invariant with time. The observable function $\log(1 + (x_{i,t}/C)^{p_i})$ can be expressed by:

$$\begin{aligned} \log\left(1 + \left(\frac{x_{i,t}}{C}\right)^{p_i}\right) &\approx \left(\frac{x_{i,t}}{C}\right)^{p_i} = \left(\frac{f_i(\mathbf{x}_{t-1})}{C}\right)^{p_i} \\ &= \frac{f_i(\mathbf{0})^{p_i}}{C^{p_i}} + \sum_{p_1, \dots, p_N \in \mathcal{P}} b_{p_1, \dots, p_N} \prod_{m \in \mathcal{N}} \left(\frac{x_{m,t-1}}{C}\right)^{p_m} \\ &\approx \frac{f_i(\mathbf{0})^{p_i}}{C^{p_i}} + \sum_{m \in \mathcal{N}, p \in \mathcal{P}} b_{m,p} \log\left(1 + \left(\frac{x_{m,t-1}}{C}\right)^p\right), \end{aligned} \quad (10)$$

where b_{p_1, \dots, p_N} and $b_{m,p}$ are coefficients invariant with time.

Given Eqs. (9)-(10), any observable functions in Eq. (7) at time t can be approximated from those at time $t-1$, via a linear matrix operator, i.e., the approximated Koopman operator denoted as \mathbf{K} :

$$\boldsymbol{\psi}(\mathbf{x}_t) = \mathbf{K} \cdot \boldsymbol{\psi}(\mathbf{x}_{t-1}). \quad (11)$$

Here, the elements of \mathbf{K} is the coefficients from Eqs. (9)-(10). As such, the approximated Koopman operator \mathbf{K} can be derived either from the theoretical deduction if the dynamic model in Eq. (1) is known, or from the simulated networked training data. We use the second method in this work, by simulating D groups of training data denoted as $\mathbf{x}_{1:\tau}^{(d)}$ with $d = 1, \dots, D$. Then, by separating the training data into two matrix as $\mathbf{Y} = [\boldsymbol{\psi}(\mathbf{x}_{2:\tau}^1), \dots, \boldsymbol{\psi}(\mathbf{x}_{2:\tau}^D)]$, and $\mathbf{X} = [\boldsymbol{\psi}(\mathbf{x}_{1:\tau-1}^1), \dots, \boldsymbol{\psi}(\mathbf{x}_{1:\tau-1}^D)]$, we train the Koopman operator \mathbf{K} via:

$$\mathbf{K} = \operatorname{argmin} \|\mathbf{Y} - \mathbf{K}\mathbf{X}\|_2^2, \quad (12)$$

where $\|\cdot\|_2$ denotes the l_2 -norm.

Compared to the existing polynomial-based observable functions for Koopman linearization in [37], the advantage of the proposed logarithm-based observable functions lies in its ability to replace the complex and substantial multi-element multiplicative observable functions with logarithm summation. This reduces the size of the observable \mathbf{z}_t from $O(N^2)$ to $O(N)$ given the comparison from Eq. (4) and Eq. (7), especially for the large-scale network with $N > 50$. By doing so, we are able to model the unknown evolution of the networked state-space via the linear Koopman operator, which now enables the analysis of optimal sensor placement using standard linear theory.

However, it is noteworthy that the direct use of linear theory [18]–[21] on Koopman linearized evolution model leads to the overlook of nonlinear dependency between the scalar-valued observable \mathbf{z}_t , as all its elements are determined by the corresponding lower-sized original state-space, i.e., $\mathbf{z}_t = \boldsymbol{\psi}(\mathbf{x}_t)$ of size M is determined by \mathbf{x}_t of size N (comprehensive explanation is given in Section V. A). As such, it is demanding to design new sampling and recovery algorithms that exploit such nonlinear dependency, and here comes the nonlinear GFT.

IV. SAMPLING WITH NONLINEAR GRAPH FOURIER TRANSFORM

In this section, we elaborate the concept and sampling theory of the nonlinear GFT which aims to capture and exploit the nonlinear dependence between observables.

A. Nonlinear GFT concept

The general concept of the GFT operator and its bandlimitedness is given as follows:

Definition 1: The general GFT operator is an invertible vector-valued function that one-to-one maps a range set \mathcal{C}_r from another set \mathcal{C}_d , where \mathcal{C}_r is called the frequency response. We call \mathcal{C}_r a bandlimited frequency response if the size of $\mathbf{x} \in \mathcal{C}_r$ is smaller than that of $\mathbf{z} \in \mathcal{C}_d$.

Here, different from the traditional linear GFT where the vector-valued function is a linear operator [17], [24]–[33], we generalize the definition which also accounts for the non-linear GFT operator.

For this work, the Koopman linearization process yields a new network with $M > N$ nodes linked by the Koopman operator \mathbf{K} , as is shown in Fig. 1(b). The indexed signals are the M constructed scalar-valued observables in $\mathbf{z}_t = \boldsymbol{\psi}(\mathbf{x}_t)$.

As such, a nonlinear GFT operator that combines the network topology and dynamic information can be assigned as the inverse of Koopman observable in Eq. (7), i.e., $\psi^{-1} : \mathcal{C}_d \rightarrow \mathbb{R}^N$. The frequency response is the original signal with the bandlimitedness property (i.e., $N < M$), which is signal-independent for any $\mathbf{z}_t \in \mathcal{C}_d$.

B. Theory of Nonlinear GFT

With the help of the generalized GFT operator, we next propose the nonlinear graph sampling theory, by providing (i) the conditions for the sampling matrix, and (ii) how to recover the signal from the samples.

Theorem 1: Given a GFT operator $\psi^{-1} : \mathcal{C}_d \rightarrow \mathcal{C}_r$, any $\mathbf{z} \in \mathcal{C}_d$, and a matrix Θ , a sampling operator (matrix) \mathbf{S}_Θ ensuring the recovery of \mathbf{z} from $\mathbf{S}_\Theta \cdot \Theta \cdot \mathbf{z}$ should maintain the one-to-one mapping characteristic of the function $\mathbf{S}_\Theta \cdot \Theta \circ \psi$. The recovered signal of \mathbf{z} , denoted as $\hat{\mathbf{z}}$ is expressed as:

$$\hat{\mathbf{z}} = \psi \left((\mathbf{S}_\Theta \cdot \Theta \circ \psi)^{-1} (\mathbf{S}_\Theta \cdot \Theta \cdot \mathbf{z}) \right) \quad (13)$$

Proof: We denote frequency response of \mathbf{z} as $\mathbf{x} \in \mathcal{C}_r$. As such, the process of GFT and inverse GFT can be expressed as:

$$\mathbf{x} = \psi^{-1}(\mathbf{z}), \quad (14)$$

$$\mathbf{z} = \psi(\mathbf{x}). \quad (15)$$

given the invertible property of the GFT operator. We then multiply the sampling matrix \mathbf{S}_Θ on both side of $\Theta \cdot \mathbf{z} = \Theta \cdot \psi(\mathbf{x})$, i.e.,

$$\mathbf{S}_\Theta \cdot \Theta \cdot \psi(\mathbf{x}) = (\mathbf{S}_\Theta \cdot \Theta \circ \psi)(\mathbf{x}) = \mathbf{S}_\Theta \cdot \Theta \cdot \mathbf{z}. \quad (16)$$

As such, equation

$$\mathbf{x} = (\mathbf{S}_\Theta \cdot \Theta \circ \psi)^{-1} (\mathbf{S}_\Theta \cdot \Theta \cdot \mathbf{z}) \quad (17)$$

holds if and only if the existence of the inverse function of $\mathbf{S}_\Theta \cdot \Theta \circ \psi$, which is equivalent to its one-to-one mapping characteristic. Then, by taking Eq. (17) into Eq. (15), the recovered signal $\hat{\mathbf{z}}$ can be computed as Eq. (13). ■

Proposition 1: Given a GFT operator $\psi^{-1} : \mathcal{C}_d \rightarrow \mathcal{C}_r$ with $\dim \mathcal{C}$, one prerequisite for signal recovery is that the number of rows of sampling matrix \mathbf{S}_Θ is no lesser than $\dim \mathcal{C}$.

Proof: Otherwise the number of rows of the sampling matrix \mathbf{S}_Θ is $\dim \mathcal{C} - 1$. Given from Theorem 1, $\mathbf{S}_\Theta \cdot \Theta \circ \psi$ is one-to-one mapping. This suggests that all $\dim \mathcal{C} - 1$ scalar-valued functions of $\mathbf{S}_\Theta \cdot \Theta \circ \psi$ constitute a set of basic functions of \mathcal{C}_r , which contradicts its dimension, i.e., $\dim \mathcal{C} \neq \dim \mathcal{C} - 1$. ■

Proposition 2: Given a GFT operator $\psi^{-1} : \mathcal{C}_d \rightarrow \mathcal{C}_r$ with $\dim \mathcal{C}$, one prerequisite for sampling matrix \mathbf{S}_Θ is that, at least $\dim \mathcal{C}$ scalar-valued functions of $\mathbf{S}_\Theta \cdot \Theta \circ \psi$ are linear independent.

Proof: Otherwise, if any $\dim \mathcal{C}$ scalar-valued functions of $\mathbf{S}_\Theta \cdot \Theta \circ \psi$ are linear dependent, then there exists $< \dim \mathcal{C}$ linear independent scalar-valued functions that constitute a set of basic function, suggesting $\dim \mathcal{C}_d = \dim \mathcal{C}_r < \dim \mathcal{C}$. ■

After the elaboration of the non-linear GFT and the rules for the sampling node selection, we next describe how this can be combined with sequential state-space information for optimal sampling and signal recovery.

C. GFT-based Linear Evolution Analysis

Recalling the Koopman linearized model in Eq. (11), linear evolution analysis aims to infer the initial observable at $t = 1$ via the samples of the later states from $1 \leq t \leq T$. Then, the unsampled signals from then remaining unsampled nodes can be reconstructed via the Koopman linearized evolution model and the inferred initial observable. We specify the Koopman linearized evolution model as follows:

$$\begin{bmatrix} \mathbf{z}_1 \\ \mathbf{z}_2 \\ \vdots \\ \mathbf{z}_\tau \end{bmatrix} = \begin{bmatrix} \mathbf{K}^0 \\ \mathbf{K}^1 \\ \vdots \\ \mathbf{K}^{\tau-1} \end{bmatrix} \cdot \mathbf{z}_1 \quad (18)$$

With the help of the non-linear GFT theory, we assign $\Theta = [(\mathbf{K}^0)^T, \dots, (\mathbf{K}^{\tau-1})^T]^T$. The GFT operator is ψ^{-1} , which maps the range set of the observable \mathbf{z}_t to \mathbf{x}_t , the original signals with $\dim \mathcal{C} = N$ indexed on N original nodes over graph $\mathcal{G}(\mathcal{N}, \mathbf{A})$. The aim then can be converted to how to determine the sampling nodes set $\mathcal{S} \subset \mathcal{N}$, and the design for recovering \mathbf{z}_1 .

1) *Selection of Sampling Nodes:* It is noteworthy that the mapping from the sampling node set $\mathcal{S} \subset \mathcal{N}$ of original network, to the sampling matrix \mathbf{S}_Θ in Theorem 1, is:

$$\mathcal{S}_\psi = \left\{ m \mid \psi_m(\mathbf{x}_t) = \psi_m(\mathbf{S} \cdot \mathbf{x}_t) \right\}, \quad (19)$$

$$\mathbf{S}_\psi = [s_{i,m_i} = 1], m_i \in \mathcal{S}_\psi, \quad (20)$$

$$\mathbf{S}_\Theta = \mathbf{S}_\psi \otimes \underbrace{[1, \dots, 1]}_\tau, \quad (21)$$

where \otimes is the Kronecker product. For convenience, we denote the above relations by

$$\mathbf{S}_\Theta = \Gamma(\mathcal{S}). \quad (22)$$

Given Theorem 1, the optimal selection of \mathcal{S} should ensure the one-to-one mapping characteristic of the function $\mathbf{S}_\Theta \cdot \Theta \circ \psi$, which is a NP-hard challenge. As such, we provide a sub-optimal requirement based on the Propositions 1-2, aiming to find $\dim \mathcal{C} = N$ linearly independent rows of Θ , i.e.,

$$\text{rank}(\Gamma(\mathcal{S}) \cdot \Theta) = N. \quad (23)$$

Here, the difference between Eq. (23) and the full column-rank sampling selection, i.e., $\text{rank}(\Gamma(\mathcal{S}) \cdot \Theta) = M > N$ will be detailed in Section V. A. We realize Eq. (23) by minimizing the quotient between the 1st and N th singulars of $\mathbf{S}_\Theta \cdot \Theta = \Gamma(\mathcal{S}) \cdot \Theta$, i.e.,

$$\mathcal{S} = \underset{\mathcal{S} \subset \mathcal{N}}{\text{argmin}} \left\{ \frac{\sigma_1(\Gamma(\mathcal{S}) \cdot \Theta)}{\sigma_N(\Gamma(\mathcal{S}) \cdot \Theta)} \right\}, \quad (24)$$

where $\sigma_i(\cdot)$ denotes the i th singular of the matrix.

Eq. (24) is implemented via a greedy algorithm in Algo. 1. The inputs are the original node set \mathcal{N} from graph $\mathcal{G}(\mathcal{N}, \mathbf{A})$, and the matrix Θ that describes the linear relations between initial observable \mathbf{z}_1 and further linear evolved observables $\mathbf{z}_{1:\tau}$. Step 1 is to initialize the sampling node set. Steps 2-5 is to greedily add node with minimum quotient between 1st and N th singulars. The output is the sampling node set \mathcal{S} indicating which nodes are selected for sampling in original graph $\mathcal{G}(\mathcal{N}, \mathbf{A})$.

Algorithm 1 Sampling Node Selection

Input: \mathcal{N}, Θ

- 1: Initialize $\mathcal{S} = \emptyset$,
- 2: **while** $\frac{\sigma_1(\Gamma(\mathcal{S}) \cdot \Theta)}{\sigma_N(\Gamma(\mathcal{S}) \cdot \Theta)} > \gamma$ **do**
- 3: $n = \operatorname{argmin}_{n \in \mathcal{N} \setminus \mathcal{S}} \left\{ \frac{\sigma_1(\Gamma(\mathcal{S} \cup \{n\}) \cdot \Theta)}{\sigma_N(\Gamma(\mathcal{S} \cup \{n\}) \cdot \Theta)} \right\}$.
- 4: $\mathcal{S} = \mathcal{S} \cup \{n\}$.
- 5: **end while**

Output: Return \mathcal{S} .

2) *Signal Recovery*: With the derivation of the sampling node set \mathcal{S} , and its relations to the matrix \mathbf{S}_Θ in Eqs. (19)-(21), we denote the samples of $[\mathbf{z}_1, \dots, \mathbf{z}_\tau]$ as:

$$\mathbf{y} = \mathbf{S}_\Theta \cdot [\mathbf{z}_1, \dots, \mathbf{z}_\tau]^T. \quad (25)$$

Then, by taking the samples in Eq. (25) into Eq. (18), and transforming the initial observable \mathbf{z}_1 into its graph frequency response, we have:

$$\mathbf{y} = \mathbf{S}_\Theta \cdot \Theta \cdot \mathbf{z}_1 = \mathbf{S}_\Theta \cdot \Theta \cdot \psi(\mathbf{x}_1). \quad (26)$$

Regarding the difficulty of computing the inverse function $(\mathbf{S}_\Theta \cdot \Theta \circ \psi)^{-1}$, we recover the signal \mathbf{x}_1 via the gradient descend method, by:

$$\hat{\mathbf{x}}_1 = \operatorname{argmin}_{\mathbf{x}_1 \in \mathbb{R}^N} \left\{ \|\mathbf{y} - \mathbf{S}_\Theta \cdot \Theta \cdot \psi(\mathbf{x}_1)\|_2^2 \right\}, \quad (27)$$

with gradient:

$$\nabla = \left(\psi(\mathbf{x}_1)^T \cdot \Theta^T \cdot \mathbf{S}_\Theta^T - \mathbf{y}^T \right) \cdot \mathbf{S}_\Theta \cdot \Theta \cdot \frac{\partial \psi(\mathbf{x}_1)}{\mathbf{x}_1}. \quad (28)$$

After the computation of $\hat{\mathbf{x}}_1$, we can derive the estimated $\hat{\mathbf{z}}_1 = \psi(\hat{\mathbf{x}}_1)$, and $\hat{\mathbf{z}}_t = \mathbf{K}^{t-1} \hat{\mathbf{z}}_1$. Then, given the selected observable function in Eq. (7), we finally compute $\hat{\mathbf{x}}_t = \psi^{-1}(\hat{\mathbf{z}}_t)$. The process is illustrated in Fig. 1(c).

V. NOVELTY COMPARED TO OTHER STATE-OF-THE-ARTS

In this section, we distinguish our proposed Log-Koopman NL-GFT, with other state-of-the-art schemes.

A. Sampling by Linear Analysis on Poly-Koopman Operator

After the derivation of Koopman linearized evolution model, i.e., $\mathbf{z}_t = \mathbf{K}\mathbf{z}_t$, one straightforward idea is to treat the set of observable as \mathbb{R}^M , and use the standard linear theory in [17]–[21], e.g., selecting sampling nodes (corresponding rows) to make $\Theta = [(\mathbf{K}^0)^T, \dots, (\mathbf{K}^{\tau-1})^T]^T$ full column-rank, or by maximizing the state energy computed by Koopman observability gramian. Specially, the latter was implemented by the work in [38], referred to as Poly-Koopman linear evolution analysis. The sampling matrix, denoted as \mathbf{W}_h , is derived as [38]:

$$\mathbf{W}_h = [\mathbf{I}_{L \times L} \ \mathbf{0}] \cdot \mathbf{V}^{-1}, \quad (29)$$

by L largest eigenvalues of $\mathbf{K} = \mathbf{V} \operatorname{diag}(\lambda_1, \dots, \lambda_M) \mathbf{V}^{-1}$ to maximize the energy of the observable reports, i.e.,

$$\begin{aligned} & \max_{\mathbf{W}_h} \sum_{t=1}^{\tau} \mathbf{z}_1^T \cdot (\mathbf{K}^t)^T \cdot \mathbf{W}_h^T \cdot \mathbf{W}_h \cdot \mathbf{K}^t \cdot \mathbf{z}_1 \\ & = \sum_{t=1}^{\tau} \mathbf{z}_1^T \cdot \operatorname{diag}(\lambda_1^{2t}, \dots, \lambda_L^{2t}, 0, \dots, 0) \cdot \mathbf{z}_1. \end{aligned} \quad (30)$$

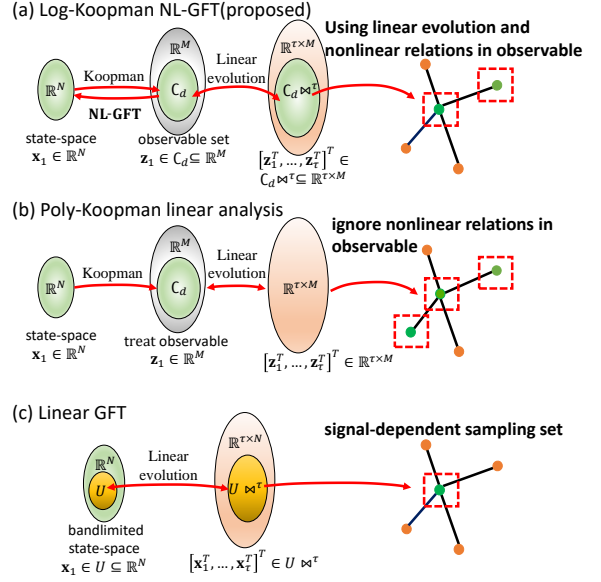


Fig. 2. Comparison of proposed Log-Koopman NL-GFT method with Poly-Koopman linear evolution analysis, and linear GFT methods. (a) gives the illustration of proposed Log-Koopman NL-GFT method, whereby the sampling node set maps from the set of NL-GFT signal-independent bandlimited frequency response, i.e., \mathbb{R}^N . (b) shows the sampling set selection from the Poly-Koopman based linear evolution analysis, whereby the initial observable set is treated as a linear space \mathbb{R}^M for linear evolution analysis, and therefore maps to redundant sampling node set. (c) shows the linear GFT, whereby the samples are selected for a specific bandlimited initial state-space, suggesting a signal-dependent sampling node selection that is not suitable for signals that are not bandlimited.

The differences lie in two aspects.

First, they used the polynomial-based observable function in Eq. (4) to linearize the networked data, which performs accurate linearization approximation for small-scale network. However, when it comes to the large-scale network (e.g., $N > 50$), they fall into the size explosion by using $O(N^2)$ terms to construct the observable function $\psi(\cdot)$, in order to ensure the linearization accuracy. We explained this by Eq. (5), and further illustration will be given in Figs. 3-4.

Second, the linear analysis on Koopman linearized evolution model overlooked the nonlinear dependency between elements in the vector-valued observable. This is because both the full column-rank condition of Θ , i.e., $\operatorname{rank}(\Gamma(\mathcal{S}) \cdot \Theta) = M > N$, and the eigenvector analysis in Eq. (29) treat the initial observable set as the linear space \mathbb{R}^M . This therefore overlooks the fact $\mathbf{z}_1 \in \mathcal{C}_r \subset \mathbb{R}^M$ with $\dim \mathcal{C}_r = N < M$, as the observable \mathbf{z}_1 is completely determined by the lower-sized $x_1 \in \mathbb{R}^N$, i.e., $\mathbf{z}_1 = \psi(\mathbf{x}_1)$. As such, the sampling node set maps from \mathbb{R}^M other than \mathcal{C}_d will inevitably result in redundant sampling node for recovering the signal \mathbf{z}_1 that belongs to \mathcal{C}_d (seen Fig. 2(a)-(b)). We show the comparison performance in Figs 5-6.

B. Comparison with Linear GFT Sampling

Linear GFT sampling method aims at sampling and recovering the networked signal \mathbf{x}_t that belong to a known subspace (also referred to as bandlimited) of \mathbb{R}^N , i.e., $\forall t \in \mathbb{N}^+, \mathbf{x}_t \in \operatorname{span}\{\mathbf{u}_1, \dots, \mathbf{u}_r\} \subset \mathbb{R}^N$. Here, the orthogonal $r < N$ vectors $\mathbf{u}_1, \dots, \mathbf{u}_r$ with $r < N$ can be derived

either from the r -leading eigenvectors of the topology-based Laplacian matrix [17], [24]–[27], or from the simulated data [11]. As such, the linear GFT operator \mathbf{U}^T can be assigned as $\mathbf{U}^T = [\mathbf{u}_1, \dots, \mathbf{u}_r]^T$, where the processes of GFT and inverse GFT are $\tilde{\mathbf{x}}_t = \mathbf{U}^T \cdot \mathbf{x}_t$ and $\mathbf{x}_t = \mathbf{U} \cdot \tilde{\mathbf{x}}_t$. The sampling matrix \mathbf{S}_Φ to ensure the recovery of \mathbf{x}_t from $\mathbf{S}_\Phi \Phi \cdot \mathbf{x}_t$ can be determined by [17], [24]–[27]

$$\text{rank}(\mathbf{S}_\Phi \cdot \Phi \cdot \mathbf{U}) = r, \quad (31)$$

where Φ can be a simple identity matrix, or $\Phi = [\mathbf{L}^0, \dots, \mathbf{L}^{T-1}]^T$ in [17] specifies the linear evolved information given $\mathbf{x}_{t+1} = \mathbf{L} \cdot \mathbf{x}_t$. Then, given \mathbf{S}_Φ and the samples $\mathbf{y} = \mathbf{S}_\Phi \Phi \cdot \mathbf{x}_t$, the recovered signal $\hat{\mathbf{x}}_t$ is [17], [24]–[27]:

$$\hat{\mathbf{x}}_t = \mathbf{U} \cdot \text{pinv}(\mathbf{S}_\Phi \cdot \Phi \cdot \mathbf{U}) \cdot \mathbf{y}, \quad (32)$$

where $\text{pinv}(\cdot)$ is the pseudo-inverse.

As is compared by Fig. 2(a) and Fig. 2(c), one difference lies in that the linear GFT sampling method is signal-dependent, since the selection of sampling set is not suitable for the signals that are not belongs to the assumed signal space. This leads to the signal-dependent sensor placement, as \mathbf{S}_Φ in Eq. (31) varies with the changes of the assumed signal space. Secondly, in the absence of any prior knowledge of the signal model or signal space, their works are unable to generate GFT operator for further network sampling and signal recovery. By contrast, our proposed Log-Koopman NL GFT captures the nonlinear bandlimitedness of the observable $\mathbf{z}_t = \psi(\mathbf{x}_t)$, which is signal-independent to any vector $\mathbf{z}_t \in \mathcal{C}_d$, therefore leading to a fixed sensor placement scheme for all signals.

VI. RESULTS

In this section, we evaluate our proposed Log-Koopman NL-GFT sampling method in terms of the size of sampling node set $|S|$, and the normalized root mean square error (N-RMSE) defined as follows:

$$\text{N-RMSE} = \sqrt{\frac{\sum_{t=1}^T (\hat{\mathbf{x}}_t - \mathbf{x}_t)^T (\hat{\mathbf{x}}_t - \mathbf{x}_t)}{\sum_{t=1}^T \mathbf{x}_t^T \mathbf{x}_t}}. \quad (33)$$

The dynamic network is configured by the Erdős-Rényi model where each edge is included in the graph with probability 0.5 that is independent from every other edge. The number of node N varies from 10 to 100. Networked data are configured by two general models with rate parameters (F , B , and R) setting according to [2], i.e.,

$$\frac{dx_i(t)}{dt} = F - B \cdot x_i - \sum_{j=1}^N R \cdot x_i \cdot x_j \quad (34)$$

$$\frac{dx_i(t)}{dt} = -B \cdot x_i + \sum_{j=1}^N R \cdot \frac{x_j^2}{1 + x_j^2} \quad (35)$$

where Eq. (34) is referred to as Biochemical Dynamics of protein-protein interactions, and Eq. (35) is referred to as gene Regulatory Dynamics. Here, it is noteworthy that we do not know the expressions of the models in Eqs. (34)–(35), but only the data generated are used for performance

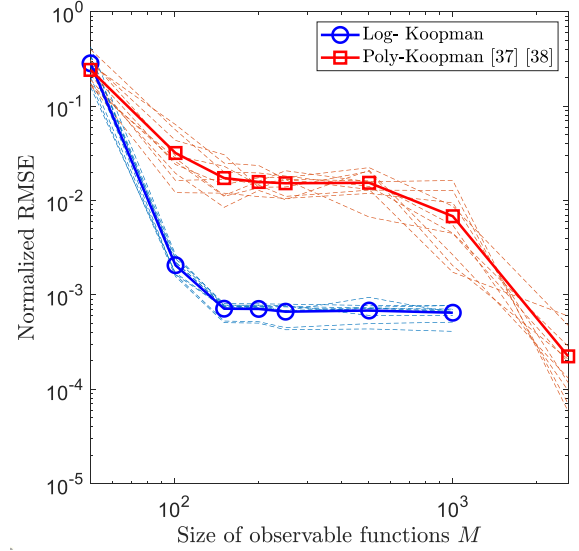


Fig. 3. Performance comparison between proposed Log-Koopman operator and Poly-based one in [37] by $N = 50$ networked data of Biochemical Dynamic of protein-protein interactions. The proposed Log-Koopman operator requires less observable functions ($M = O(N) = 250$) to approximate the original data, as opposed to the Poly-Koopman operator requiring $O(N^2) = 2500$.

evaluation. The compared algorithms are the polynomial-based Koopman operator in [37], and the work in [38] that directly used the linear evolution analysis based on the Poly-Koopman linearized model.

A. Log-Koopman Linearization Performance

We at first test the linearization performance of our proposed logarithm-based Koopman operator in Figs. 3-4. The x-coordinate illustrates the number of selected scalar-valued observable functions (i.e., ψ_1, \dots, ψ_M) used for generating the vector-valued observable function $\psi(\cdot)$ in Eq. (3). The y-coordinate gives the corresponding N-RMSE between the linearized data and the original data.

Figs. 3-4 show the linearized performance of data generated from Biochemical Dynamic of protein-protein interactions, and of gene Regulatory Dynamic data, where the number of nodes in corresponding networks are $N = 50$ and $N = 100$ respectively. It is seen that the proposed Log-based Koopman operator can reach a small N-RMSE, by using only $M = O(N)$ (e.g., $M = 3 \times N = 150$ in Fig. 3) observable functions. Such number is much lower than that of the Poly-based Koopman operator which requires $O(N^2)$. The reason is attributed to the conversion of the multiplicative terms of Taylor expansion in Eq. (4), to the form of logarithm summations in Eq. (7). As such, only definite number of logarithm-based observable functions are required to approximate and replace the indefinite multiplicative Poly-based observable functions. This suggests the ability of the proposed scheme to prevent the size explosion when linearizing large-scale networked data (i.e., $N > 50$), and therefore enables the computational feasibility of further signal processing steps relying on Koopman operator (e.g., the sampling node selection in Algo. 1).

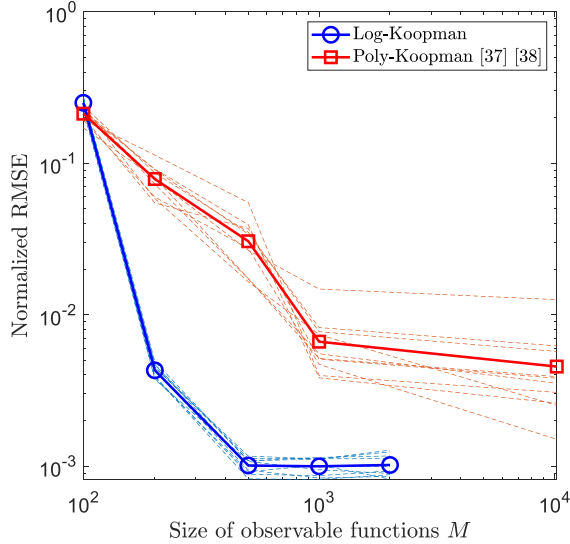


Fig. 4. Performance comparison between proposed Log-Koopman operator and Poly-based one in [37] by $N = 100$ gene Regulatory Dynamic networked data. The proposed Log-Koopman operator requires less observable functions ($M = O(N) = 10^3$) to approximate the original data, as opposed to the Poly-Koopman operator ($O(N^2) > 10^4$).

One drawback of the proposed Log-Koopman operator lies in the existence of N-RMSE lower-bound (e.g., 10^{-3} in Figs. 3-4), due to inaccuracy of the logarithm approximation of the multiplicative polynomial terms. Nevertheless, it is noteworthy that such inaccuracy is tolerable when analyzing the sampling and recovery issues of networked data, as it brings negligible N-RMSE of the recovered data. We will show this in next part.

B. Performance of Log-Koopman NL-GFT Sampling and Recovery

We then evaluate the sampling and recovery performance of the proposed NL-GFT scheme leveraged on the Log-based Koopman operator. Fig. 5 provides one illustration of the recovery N-RMSE versus the changes of the selected sampling node set $|\mathcal{S}|$ by Algo. 1, when the network has $N = 50$ nodes. It is observed that the number of selected nodes from the proposed NL-GFT scheme is much smaller than that of the competitive one in [38]. The proposed scheme can approach an order of 10^{-3} N-RMSE by using only half of nodes for sampling, as opposed to the scheme in [38] which requires nearly all nodes to ensure the recovery performance.

This can be further demonstrated in Fig. 6, where the x-coordinate represents the increase of the network size (from $N = 10$ to $N = 100$), and the y-coordinate gives the minimum size of the sampling node set $|\mathcal{S}|$ that keeps the N-RMSE of recovery in the order of 10^{-3} . We can see that with the increases of the network size N , our proposed NL-GFT scheme requires only lower than half of nodes for sampling, which is smaller than that of the competitive scheme in [38] that needs almost all the nodes.

We explain such sampling node reduction in the following. After the Koopman linearization, the original N networked data \mathbf{x}_t is expanded by the selected $M > N$ observable functions as

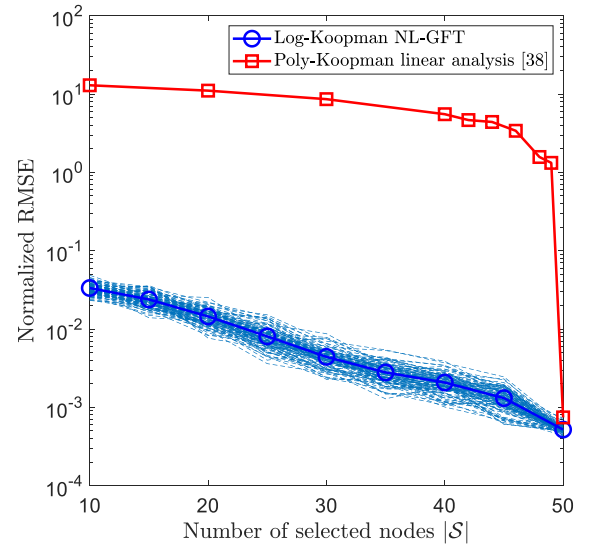


Fig. 5. One illustration of proposed Log-Koopman NL-GFT sampling scheme performance in $N = 50$ network, where x-coordinate is the number of selected sampling nodes $|\mathcal{S}|$, and y-coordinate is the N-RMSE. The proposed scheme requires $|\mathcal{S}| = 25$ sampling node to ensure an order of 10^{-3} recovery N-RMSE. The number is lower than that of the competitive algorithm in [38].

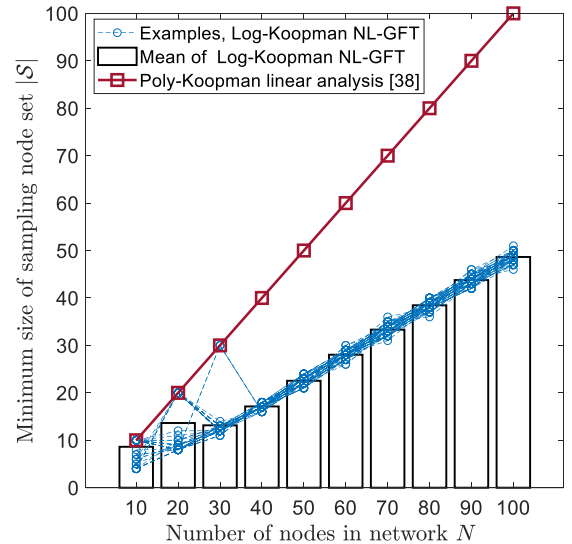


Fig. 6. Performance of proposed Log-Koopman NL-GFT sampling scheme performance, where x-coordinate is number of nodes in different networks, and y-coordinate is the minimum number of sampling node set to ensure $N - RMSE = O(10^{-3})$. With the increases of the nodes of different networks, the proposed scheme requires $|\mathcal{S}| = 0.5 \times N$ sampling node, smaller than that of the competitive algorithm in [38].

$\mathbf{z}_t = [\psi_1(\mathbf{x}_t), \dots, \psi_M(\mathbf{x}_t)]^T$, and the aim is converted to find the sampling node to recover the initial state \mathbf{z}_1 from Eq. (18). As such, the design of the sampling node selection should take into account the nonlinear dependence between the element of \mathbf{z}_1 . The linear evolution analysis in [38] treats the set of observable \mathbf{z}_1 as \mathbb{R}^M , and ignores such nonlinear dependence, thereby leading to redundant sampling nodes. By contrast, our proposed nonlinear GFT sampling method transforms the observable set to its bandlimited set of frequency response, therefore capable of deriving the smaller number of sampling

nodes mapping from a lower sized frequency response.

VII. CONCLUSION

Networked nonlinear dynamics underpin the complex functionality of many engineering, social, biological, and ecological systems. Monitoring the network's dynamics via subset of nodes is essential for a variety of operational and scientific purposes. For arbitrarily large graphs with nonlinear dynamics, current model-driven methods are dependent on the underlying model assumptions, and data-dependent sampling node selection suffer from either complexity explosion issues or lack of guarantees in performance. One state-of-the-art scheme uses a polynomial based Koopman operator to generate a linear evolution of observable defined on the original networked state-space, but the sampling node set are still large due to (i) the size explosion of poly-based observables, and (ii) the overlook of nonlinear dependence between observable.

In this work, we propose a novel logarithm based Koopman operator coupled with a novel nonlinear Graph Fourier Transform (GFT) scheme, entitled as Log-Koopman NL-GFT, for sampling and recovering the networked dynamics. The Log-Koopman operator is able to prevent the size explosion, as logarithm-form observables are designed to replace the substantial multi-element multiplicative poly-observables by logarithm summation. When combined with our novel nonlinear GFT sampling approach, our sampling node set can be completely determined by a bandlimited frequency space **in a nonlinear manner**. As such, the sampling and recovering algorithms are designed by exploiting the nonlinear dependence of observables.

The results shows that the proposed Log-Koopman NL-GFT scheme is able to (i) linearize unknown nonlinear dynamics using $O(N)$ observables, and (ii) achieve lower number of sampling nodes, compared with the state-of-the art polynomial Koopman scheme using only the linear evolution analysis, which suggests a promising prospect of the proposed Log-Koopman NL-GFT scheme to a wide range of network monitoring applications.

REFERENCES

- [1] S. Krishnagopal, J. Lehnert, W. Poel, A. Zakharova, and E. Schöll, "Synchronization patterns: From network motifs to hierarchical networks," *Philos. Trans. R. Soc. A.*, vol. 375, no. 2088, p. 20160216, Mar. 2017.
- [2] B. Barzel and A.-L. Barabási, "Universality in network dynamics," *Nat. Phys.*, vol. 9, no. 10, p. 673, Oct. 2013.
- [3] A. Wilson, "Boltzmann, lotka and volterra and spatial structural evolution: An integrated methodology for some dynamical systems," *J. Roy. Soc. Interface*, vol. 5, no. 25, pp. 865–871, Dec. 2007.
- [4] S. Dhamal, R. D. Vallam, and Y. Narahari, "Modeling spread of preferences in social networks for sampling-based preference aggregation," *IEEE Trans. Netw. Sci. Eng.*, vol. 6, no. 1, pp. 46–59, Jan. 2019.
- [5] M. Bardoscia, S. Battiston, F. Caccioli, and G. Caldarelli, "Pathways towards instability in financial networks," *Nat. Commun.*, vol. 8, p. 14416, Feb. 2017.
- [6] B. Schäfer, D. Witthaut, M. Timme, and V. Latora, "Dynamically induced cascading failures in power grids," *Nat. Commun.*, vol. 9, no. 1, p. 1975, May 2018.
- [7] X. Lu, C. Gray, L. E. Brown, M. E. Ledger, A. M. Milner, R. J. Mondragón, G. Woodward, and A. Ma, "Drought rewires the cores of food webs," *Nat. Clim. Change*, vol. 6, no. 9, p. 875, Sep. 2016.
- [8] Y. Hasegawa, "Thermodynamics of collective enhancement of precision," *Phys. Rev. E*, vol. 98, no. 3, p. 032405, Sep. 2018.
- [9] I. Scholtes, N. Wider, R. Pfitzner, A. Garas, C. J. Tessone, and F. Schweitzer, "Causality-driven slow-down and speed-up of diffusion in non-Markovian temporal networks," *Nat. Commun.*, vol. 5, p. 5024, Sep. 2014.
- [10] C. Ellinas, N. Allan, and A. Johansson, "Dynamics of organizational culture: Individual beliefs vs. social conformity," *PLoS ONE*, vol. 12, no. 6, p. e0180193, Jun. 2017.
- [11] Z. Wei, A. Pagani, G. Fu, I. Guymer, W. Chen, J. A. McCann, and W. Guo, "Optimal sampling of water distribution network dynamics using graph fourier transform," *IEEE Transactions on Network Science and Engineering*, pp. 1–1, 2019.
- [12] Z. Wei, A. Pagani, B. Li, and W. Guo, "Monitoring embedded flow networks using graph fourier transform enabled sparse molecular relays," *IEEE Communications Letters*, pp. 1–1, 2020.
- [13] J. Gao, B. Barzel, and A. Barabasi, "Universal resilience patterns in complex networks," *Nature*, vol. 530, 2016.
- [14] G. W. Moutsinas, G., "Node-Level Resilience Loss in Dynamic Complex Networks," *Nature Scientific Reports*, vol. 10, 2020.
- [15] S. Joshi and S. Boyd, "Sensor selection via convex optimization," *IEEE Transactions on Signal Processing*, vol. 57, no. 2, pp. 451–462, 2009.
- [16] J. Mei and J. M. F. Moura, "Signal processing on graphs: Causal modeling of unstructured data," *IEEE Transactions on Signal Processing*, vol. 65, no. 8, pp. 2077–2092, 2017.
- [17] E. Isufi, P. Banelli, P. Di Lorenzo, and G. Leus, "Observing and tracking bandlimited graph processes," *arXiv preprint arXiv:1712.00404*, 2017.
- [18] Y. Xue, S. Pequito, J. R. Coelho, P. Bogdan, and G. J. Pappas, "Minimum number of sensors to ensure observability of physiological systems: A case study," in *2016 54th Annual Allerton Conference on Communication, Control, and Computing (Allerton)*, 2016, pp. 1181–1188.
- [19] H. Zhang, R. Ayoub, and S. Sundaram, "Sensor selection for kalman filtering of linear dynamical systems: Complexity, limitations and greedy algorithms," *Automatica*, vol. 78, pp. 202–210, 2017.
- [20] S. Pequito, P. Bogdan, and G. J. Pappas, "Minimum number of probes for brain dynamics observability," in *2015 54th IEEE Conference on Decision and Control (CDC)*, 2015, pp. 306–311.
- [21] F. S. Cattivelli and A. H. Sayed, "Diffusion strategies for distributed kalman filtering and smoothing," *IEEE Transactions on Automatic Control*, vol. 55, no. 9, pp. 2069–2084, 2010.
- [22] N. D. Sidiropoulos and A. Kyrillidis, "Multi-way compressed sensing for sparse low-rank tensors," *IEEE Signal Process. Lett.*, vol. 19, no. 11, pp. 757–760, Nov. 2012.
- [23] X. Ding, W. Chen, and I. J. Wassell, "Joint sensing matrix and sparsifying dictionary optimization for tensor compressive sensing," *IEEE Trans. Signal Process.*, vol. 65, no. 14, pp. 3632–3646, Jul. 2017.
- [24] S. Chen, R. Varma, A. Sandryhaila, and J. Kovacevic, "Discrete signal processing on graphs: Sampling theory," *IEEE Trans. Signal Process.*, vol. 63, no. 24, pp. 6510–6523, Dec. 2015.
- [25] A. Anis, A. Gadde, and A. Ortega, "Efficient sampling set selection for bandlimited graph signals using graph spectral proxies," *IEEE Trans. Signal Process.*, vol. 64, no. 14, pp. 3775–3789, Jul. 2016.
- [26] S. Chen, R. Varma, A. Singh, and J. Kovacevic, "Signal recovery on graphs: Fundamental limits of sampling strategies," *IEEE Trans. Signal Inf. Process. over Networks*, vol. 2, no. 4, pp. 539–554, Dec. 2016.
- [27] A. Ortega, P. Frossard, J. Kovacevic, J. M. F. Moura, and P. Vandergheynst, "Graph signal processing: Overview, challenges, and applications," *Proc. IEEE*, vol. 106, no. 5, pp. 808–828, May 2018.
- [28] D. Romero, V. N. Ioannidis, and G. B. Giannakis, "Kernel-based reconstruction of space-time functions on dynamic graphs," *IEEE Journal of Selected Topics in Signal Processing*, vol. 11, no. 6, pp. 856–869, 2017.
- [29] P. Di Lorenzo, S. Barbarossa, P. Banelli, and S. Sardellitti, "Adaptive least mean squares estimation of graph signals," *IEEE Transactions on Signal and Information Processing over Networks*, vol. 2, no. 4, pp. 555–568, 2016.
- [30] P. Di Lorenzo, P. Banelli, S. Barbarossa, and S. Sardellitti, "Distributed adaptive learning of graph signals," *IEEE Transactions on Signal Processing*, vol. 65, no. 16, pp. 4193–4208, 2017.
- [31] S. Segarra, A. G. Marques, G. Leus, and A. Ribeiro, "Reconstruction of graph signals through percolation from seeding nodes," *IEEE Transactions on Signal Processing*, vol. 64, no. 16, pp. 4363–4378, 2016.
- [32] M. Tsitsvero, S. Barbarossa, and P. Di Lorenzo, "Signals on graphs: Uncertainty principle and sampling," *IEEE Transactions on Signal Processing*, vol. 64, no. 18, pp. 4845–4860, 2016.
- [33] F. Grassi, A. Loukas, N. Perraudin, and B. Ricaud, "A time-vertex signal processing framework: Scalable processing and meaningful representations for time-series on graphs," *IEEE Transactions on Signal Processing*, vol. 66, no. 3, pp. 817–829, 2018.

- [34] M. O. Williams, I. G. Kevrekidis, and C. W. Rowley, "A data-driven approximation of the koopman operator: Extending dynamic mode decomposition," *Journal of Nonlinear Science*, vol. 25, no. 6, pp. 1307–1346, 2015.
- [35] M. A. Hernández-Ortega and A. R. Messina, "Nonlinear power system analysis using koopman mode decomposition and perturbation theory," *IEEE Transactions on Power Systems*, vol. 33, no. 5, pp. 5124–5134, 2018.
- [36] M. Netto and L. Mili, "A robust data-driven koopman kalman filter for power systems dynamic state estimation," *IEEE Transactions on Power Systems*, vol. 33, no. 6, pp. 7228–7237, 2018.
- [37] E. Yeung, Z. Liu, and N. O. Hodas, "A koopman operator approach for computing and balancing gramians for discrete time nonlinear systems," in *2018 Annual American Control Conference (ACC)*, 2018, pp. 337–344.
- [38] A. Hasnain, N. Boddupalli, and E. Yeung, "Optimal reporter placement in sparsely measured genetic networks using the koopman operator," in *2019 IEEE 58th Conference on Decision and Control (CDC)*, 2019, pp. 19–24.